Available online at www.sciencedirect.com
ScienceDirect
Trans. Nonferrous Met. Soc. China 25(2015) 2986−2993
Transactions of Nonferrous Metals Society of China
www.tnmsc.cn

Pd micro-nanoparticles electrodeposited on graphene/polyimide membrane for electrocatalytic oxidation of formic acid

Yan ZHANG, Qin WANG, Wei-chun YE, Jia-jia LI, Chun-ming WANG

College of Chemistry and Chemical Engineering, Lanzhou University, Lanzhou 730000, China

Received 29 October 2014; accepted 28 May 2015

Abstract: A novel Pd electrocatalyst with flowerlike micro-nanostructures was synthesized by electrochemical deposition on a flexible graphene/polyimide (Gr/PI) composite membrane and characterized by scanning electron microscopy (SEM), X-ray diffraction (XRD). The Pd micro-nanoparticles were prepared on a COOH-CNTs/PI membrane as a comparative sample. The XRD and SEM investigations for Pd electrodeposition demonstrate that the particle size of Gr/PI composite membrane is smaller than that of COOH-CNTs/PI membrane, while the uniform and dense distribution of Pd micro-nanoparticles on the Gr/PI composite membrane is greater than that on the COOH-CNTs/PI membrane. The electrocatalytic properties of Pd/Gr/PI and Pd/COOH-CNTs/PI catalysts for the oxidation of formic acid were investigated by cyclic voltammetry (CV) and chronoamperometry (CA). It is found that the electrocatalytic activity and stability of Pd/Gr/PI are superior to those of Pd/COOH-CNTs/PI catalyst. This is because smaller metal particles and higher dense distribution desirably provide abundant catalytic sites and mean higher catalytic activity. Therefore, the Pd/Gr/PI catalyst has better catalytic performance for formic acid oxidation than the Pd/COOH-CNTs/PI catalyst.

Key words: Pd micro-nanoparticles; graphene/polyimide membrane; carboxyl carbon nanotubes/polyimide membrane; electro catalytic oxidation; formic acid; electrochemical deposition

1 Introduction

Recently, Pd-based nanomaterials are extensively used as anode electrocatalysts to catalyze formic acid oxidation in direct formic acid fuel cells (DFAFCs) [1−3]. However, the poor durability/stability of conventional Pd electrocatalysts has become a major obstacle for the commercialization of the DFAFC technology [4,5]. Although the reasons for the poor durability of Pd catalysts in DFAFCs are still not fully clear, some possibilities have been proposed: the aggregation of Pd micro-nanoparticles, the fast dissolution of Pd from the carbon support under the DFAFCs operating conditions, and CO accumulation at relatively high formic acid concentrations [4,5]. These difficulties warrant the development of highly durable and efficient Pd-based electrocatalysts for DFAFCs application.

The nanocomposite membrane based on carbon nanotubes (CNTs) and aromatic polyimides (PIs) is found to be an excellent support for loading electrocatalysts [6−8]. The membrane exhibits the excellent electrical property, chemical stability and high specific surface area of CNTs and the excellent thermal stability, dimensional stability, and mechanical properties of PIs [9−13]. However, in comparison with CNTs, grapheme (Gr), one-atom thick planar sheet of hexagonally arrayed sp^2 carbon atoms, has attracted tremendous scientific attention in recent years [14−19]. This two-dimensional (2D) material exhibits excellent physical and chemical properties, which makes it promising for potential applications in many technological fields, such as nanoelectronics, sensors, nanocomposites, batteries, supercapacitors and hydrogen storage [14]. Especially, graphene has potential application as a heterogeneous catalyst support in direct methanol fuel cells [20−23]. Additionally, the production cost of Gr in large quantities is much lower than that of CNTs [17,24]. So the Gr/PI material as substrate is believed to represent better corrosion resistance and chemical stability, higher specific surface area, enhanced mechanical performance and endurance of high potential (vs SCE) at low pH (pH<1) [13,25−28] than the CNTs/PI.

Foundation item: Project (51372106) supported by the National Natural Science Foundation of China
Corresponding author: Chun-ming WANG; Tel: +86-931-8912596; Fax: +86-931-8912582; E-mail: wangcm@lzu.edu.cn
DOI: 10.1016/S1003-6326(15)63925-5

This work describes the preparation, characterization and electrocatalytic applications of Pd micro-nanoparticles electrodeposited on the Gr/PI nanocomposite membrane. The obtained film is slim, light and flexible, which makes it easily processed and recycled. The as-prepared Pd/Gr/PI catalyst shows higher electrocatalytic activity and stability than Pd/COOH-CNTs/PI.

2 Experimental

2.1 Materials

4,4-oxydianiline (ODA) and 4,4-oxydiphthalic anhydride (ODPA) were purchased from Shanghai Chemical (Shanghai, China). N-methyl pyrrolidone (NMP) was redistilled. $PdCl_2$ was purchased from Sigma Aldrich Reagent Company and carboxyl carbon nanotubes (COOH-CNTs) were purchased from Chengdu Science and Technological Company. Graphene was synthesized by a modified Hummers and Offeman's method [29].

2.2 Preparation of Gr/PI membrane

The preparation of Gr/PI membrane was as follows (Fig. 1). Firstly, a 1:1 molar ratio of ODA and ODPA were added into anhydrous NMP solvent and stirred for 24 h in the magnetic stirrer to obtain polyamic acid (PAA). Then, graphene was added into PAA solution and stirred fully. Thirdly, the solution containing graphene was paved onto a glass slide. Finally, the slide was evaporated at 60 °C for 3 h and sequentially heated up to 250 °C in 200 min. The Gr/PI membrane was obtained via separating from the glass slide. The COOH-CNTs/PI membrane was obtained under the same conditions.

2.3 Preparation of Pd/Gr/PI

Pd micro-nanoparticles were electrodeposited on the Gr/PI membrane in the aqueous solution of 5 mmol/L $PdCl_2$ + 0.1 mol/L NaCl. The deposition potential was 0.2 V and the deposition time was selected as 1000 s. The water was purified by Milli-Q pure water system (Millipore, electrical resistivity of 18.2 MΩ/cm). The Pd/COOH-CNTs/PI was prepared under the same process.

2.4 Characterization

The crystal structures of samples were identified by X-ray diffraction (XRD, RigakuD/Max−2400). The morphology and size of the material were characterized by field emission scanning electron microscopy (FE-SEM, Hitachi S−944800, Japan).

2.5 Electrochemical measurements

The electrochemical properties of the samples were measured by cyclic voltammetry in a standard three-electrode cell using A CHI 612E electrochemical workstation at room temperature. The as-prepared Gr/PI membrane was used as the working electrode. The preparation method of the working electrode has been detailed in the previous work [6,30]. A Pt wire was used as the counter electrode and a saturated calomel electrode (SCE) was used as the reference electrode. To measure the formic acid electrooxidation reaction activity, cyclic voltammetry was performed between −0.2 and +0.8 V in a mixing solution containing 0.5 mol/L HCOOH and 0.5 mol/L H_2SO_4. The scan rate

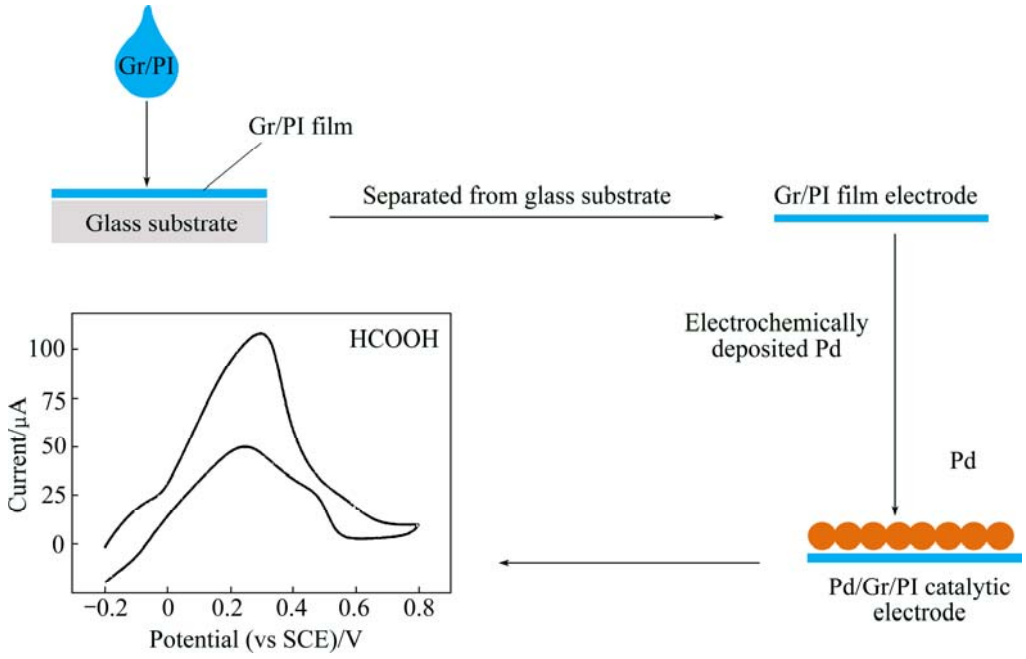

Fig. 1 Schematic of fabrication and electrocatalytic application of Pd/Gr/PI film electrode

was set as 50 mV/s. And to evaluate the catalytic stability of catalysts, the chronoamperometry (CA) experiments were carried out in the solution of 0.5 mol/L H_2SO_4 + 0.5 mol/L HCOOH at a constant potential of 0.3 V.

3 Results and discussion

3.1 SEM and XRD analyses

Figures 2(a) and (c) show the surface morphology of COOH-CNTs/PI membrane and Gr/PI membrane, respectively. It can be observed that COOH-CNTs and Gr are dispersed uniformly in PI, what is more, the films' surface are relatively flat. Controlling the size and dispersion of Pd micro-nanoparticles on the COOH-CNTs/PI and Gr/PI composite membrane is critical for their application in fuel cells [31]. The SEM analysis reveals that well defined flowerlike micro-nanostructure Pd particles, 0.9−1.2 μm in diameter, are uniformly dispersed on the COOH-CNTs/PI composite membrane surface (Fig. 2(b)). For Pd particles electrodeposited on the Gr/PI composite membrane surface, the particle size is from 0.5 to 0.85 μm (Fig. 2(d)). And the uniform and dense distribution of smaller Pd micro-nanoparticles on the Gr/PI composite membrane is greater than those on the COOH-CNTs/PI membrane. Therefore, the Gr/PI composite membrane is proved to be a better catalyst support than the COOH-CNTs/PI membrane.

Figure 3 shows the typical XRD patterns of Pd/COOH-CNTs/PI and Pd/Gr/PI catalysts, COOH-CNTs/PI and Gr/PI membranes. The diffraction peak observed at ~24.7° is attributed to the carbon materials. Furthermore, the diffraction peaks at 40°, 47°, 68°, 83° and 86° correspond to the Pd (111), (200), (220), (311) and (222) planes, respectively, which proves the typical character of a crystalline Pd face-centered cubic (FCC) pattern [32−37]. The XRD patterns indicate that Pd micro-nanoparticles electrodeposited on the two samples are both FCC crystals, while the peak intensity on the Gr/PI electrode is greater than that on the COOH-CNTs/PI electrode.

3.2 Electrochemical behaviors of Pd electrodeposition

The effect of the membrane on the Pd electrodeposition was investigated by cyclic voltammograms (CV) and chronoamperometic curve. Figure 4 shows the CV curves of the COOH-CNTs/PI and Gr/PI membranes electrodes in 0.1 mol/L NaCl and 5 mmol/L $PdCl_2$ solution at a scan rate of 10 mV/s. It can be seen that there are three coupled reduction−oxidation peaks on the COOH-CNTs/PI and Gr/PI membrane electrodes. A couple of reduction−oxidation peaks C1 and A1 belong to the reduction and oxidation of Pd, respectively. Also, the reduction of Pd starts from 0.45 V to peak C1 until the maximum peak current, and the cathode current achieves limiting diffusion current density and maintains stable until about 0.1 V. Another pair of slightly smaller peaks C2 and A2 should be attributed to the adsorption and desorption process of chloride ion. The most negative position of the pair of reduction−oxidation peaks C3 and A3 should be attributed to the adsorption and desorption process of H on Pd metal [38−40]. It is known that in the process of

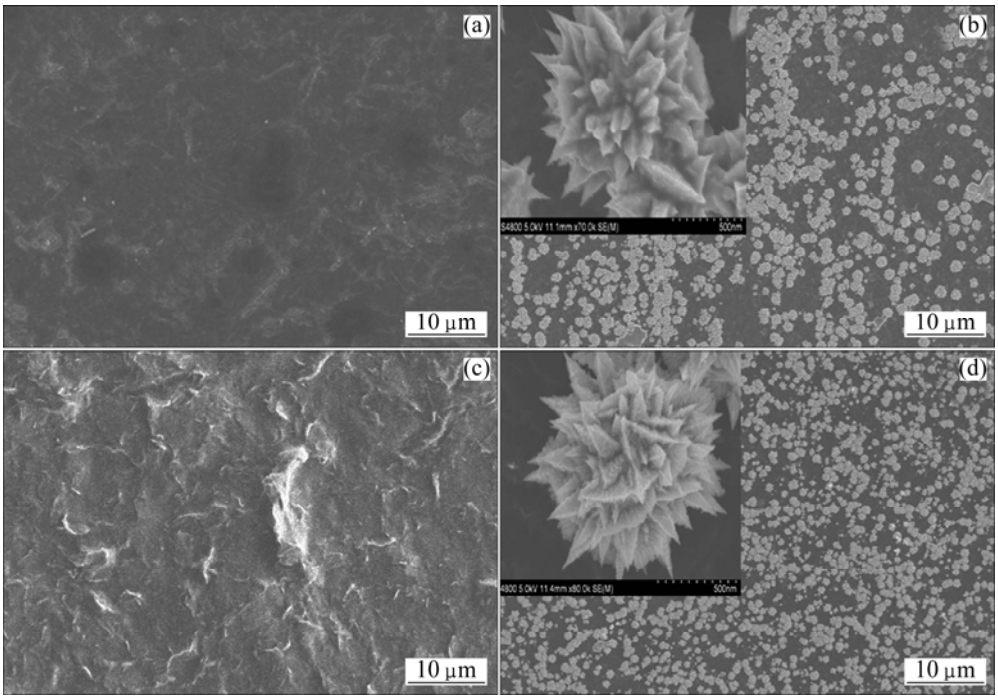

Fig. 2 SEM images of blank COOH-CNTs/PI composition membrane (a), Pd catalysts electrodeposited on COOH-CNTs/PI membrane (b), blank Gr/PI composition membrane (c) and Pd catalysts electrodeposited on Gr/PI membrane (d)

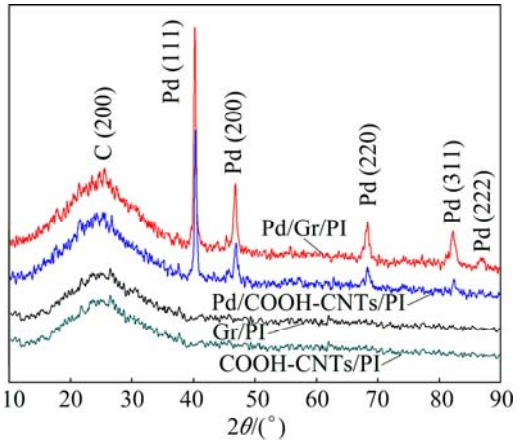

Fig. 3 XRD patterns of Pd nanoflowers on COOH-CNTs/PI and Gr/PI membrane and their blank membranes

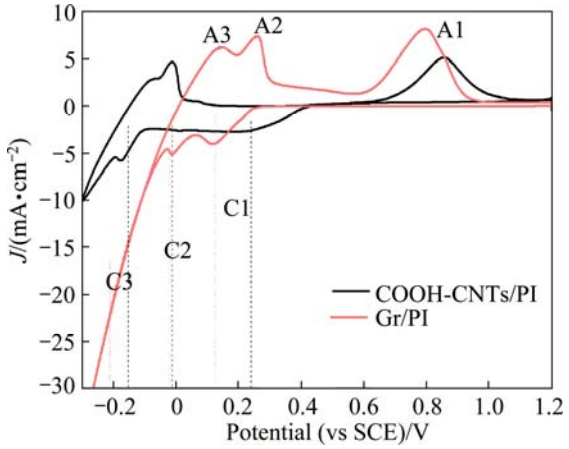

Fig. 4 CV curves measured for COOH-CNTs/PI and Gr/PI electrode in 0.1 mol/L NaCl +5 mmol/L $PdCl_2$ solution at scan rate of 10 mV/s

electrochemical deposition and dissolution of Pd on Pt and Au single crystal, $PdCl_4^{2-}$ complex is very important [41,42], and the asymmetry of three coupled peaks is caused by the chloride ion and $PdCl_4^{2-}$ complex adhering on Pd in the solution [43]. However, the relative negative shift of all reduction−oxidation peaks on Gr/PI electrode is caused by the differences of electrode surface. Besides, the current density on the Gr/PI electrode is greater than that on the COOH-CNTs/PI electrode due to the better conductivity of graphene.

Various studies on the electrodeposited metals have shown that the shift of the growth process, from progressive to instantaneous, is brought about by a more negative potential for the electrolysis. According to the CV data of different electrodes shown in Fig. 4, the potential of 0.2 V (vs SCE) was chosen for the Pd electrochemical deposition. According to the model including diffusion-controlled growth of hemispherical particles proposed by SCHARIFKER and HILLS [44], the deposition transients for progressive and instantaneous nucleation can be described by the equations:

$$\left(\frac{J}{J_{\max}}\right)^2_{\text{instantaneous}} = 1.9524\left(\frac{t}{t_{\max}}\right)^{-1}\left\{1-\exp\left[-1.2564\left(\frac{t}{t_{\max}}\right)\right]\right\}^2 \quad (1)$$

$$\left(\frac{J}{J_{\max}}\right)^2_{\text{progressive}} = 1.2254\left(\frac{t}{t_{\max}}\right)^{-1}\left\{1-\exp\left[-2.3367\left(\frac{t}{t_{\max}}\right)^2\right]\right\}^2 \quad (2)$$

Figure 5 shows the dimensionless $(J/J_{\max})^2$ versus $t/t_{\max}$ plot and the theoretical curves of Pd electrodeposition in 0.1 mol/L NaCl + 5 mmol/L $PdCl_2$ solution on the Gr/PI electrode ($J_{\max}$=0.135 mA, $t_{\max}$= 4.2 s) and COOH-CNTs/PI electrode ($J_{\max}$=0.129 mA, $t_{\max}$=4.8 s). It is clearly seen that the current transient on the Pd/COOH-CNTs/PI electrode and Pd/Gr/PI electrode correspond to the model involving instantaneous nucleation. Because the surface of COOH-CNTs has much attachment points which benefits for the nucleation of atoms and increases the nucleation rate at the initial stage. The current transient on Pd/Gr/PI fits relatively well with the theoretical curve for instantaneous nucleation.

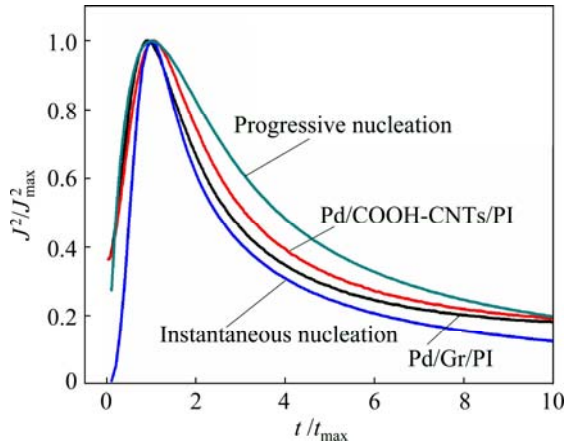

Fig. 5 Dimensionless current transients for chronoamperometic deposition of Pd micro-nanoparticles on Gr/PI electrode and COOH-CNTs/PI electrode in 0.1 mol/L NaCl +5 mmol/L $PdCl_2$ solution at 0.2 V (t=1000 s)

3.3 Electro-oxidation of formic acid

Figures 6(a) and (c) show the CVs of Pd catalyst on the COOH-CNTs/PI and Gr/PI electrodes, respectively, in 0.5 mol/L H_2SO_4 solution at a scan rate range of 10−90 mV/s. It is evident that the Pd/COOH-CNTs/PI catalyst shows the oxidation peak A1 and the reduction

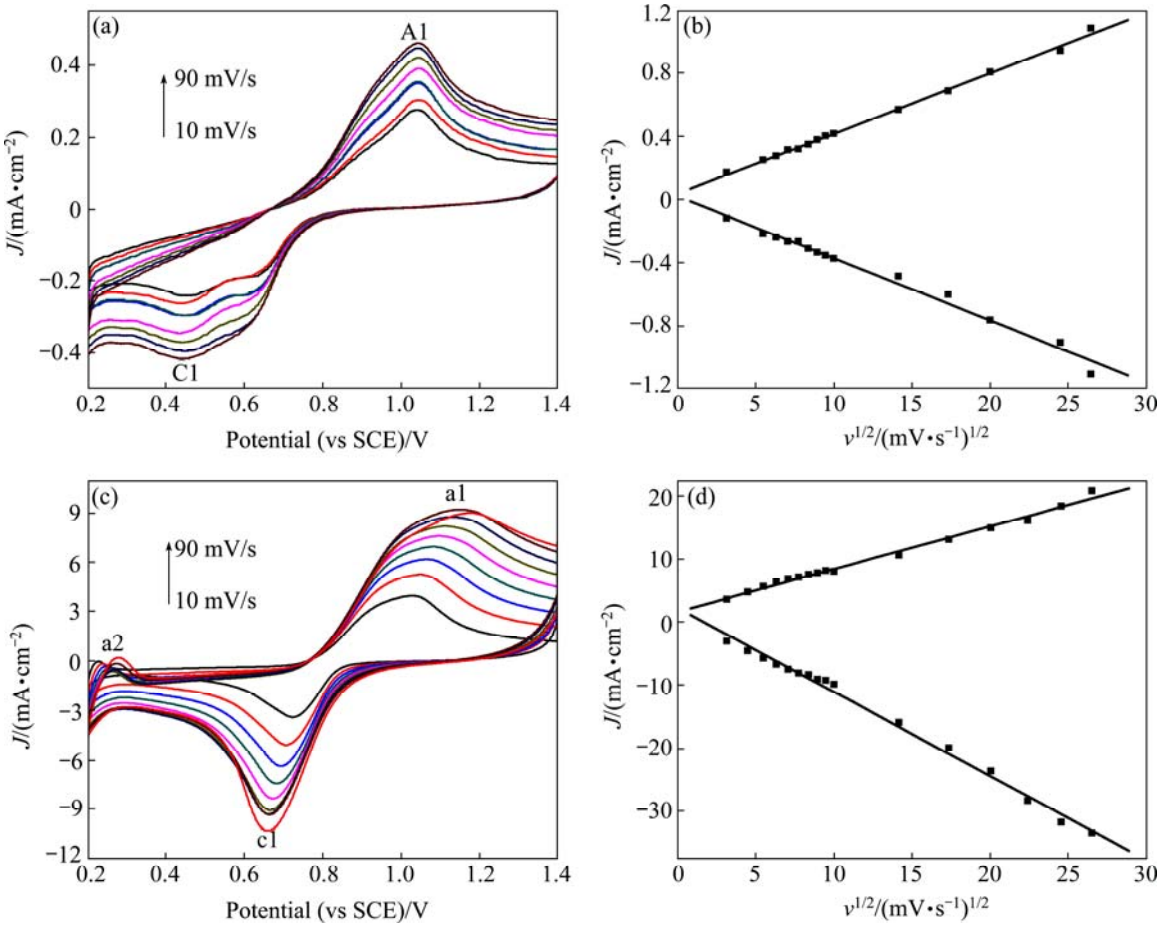

Fig. 6 Cyclic voltammograms of Pd/COOH-CNTs/PI (a) and Pd/Gr/PI (c) electrodes in 0.5 mol/L H_2SO_4 solution at different scan rates, dependency of anodic and cathodic peak currents to square root of scan rates of Pd/COOH-CNTs/PI (b) and Pb/Cr/PI (d) electrodes

peak C1 of the Pd. The Pd/Gr/PI catalyst shows the oxidation peak a1 and the reduction peak c1 of the Pd and the hydrogen adsorption (H_{ad}) peak a2. According to the calculation, the obtained results are shown in Figs. 6(b) and (d). The peak current increases linearly with the square root of the scan rates. This indicates that the electrocatalytic oxidation of formic acid on the Pd/COOH-CNTs/PI and Pd/Gr/PI electrodes is a diffusion-controlled process in 0.5 mol/L H_2SO_4 [45]. The catalytic area of Pd catalyst electrodeposited on the electrode is theoretically calculated by the following equation [46]:

$$\tau^* = \frac{4RTI_p}{vAn^2F^2} \quad (3)$$

where R is the gas constant (8.314 J/(K·mol)), T is the experimental temperature, I_p refers to the peak current, v is the scan speed, A refers to the catalytic electrode area (here for 9 mm^2), n refers to the electron transfer number in the process of reduction, and F is the Faraday constant. The τ^* values of Pd/COOH-CNTs/PI and Pd/Gr/PI are calculated to be 1.24×10^{-9} and 1.24×10^{-8} mol/cm^2, respectively. This indicates that the Pd/Gr/PI has higher electrode catalytic activity than the Pd/COOH-CNTs/PI. It is accessible that Pd micro-nanoparticles on the Gr/PI are more efficient catalysts in comparison with that on the COOH-CNTs/PI used as the catalyst support.

Figure 7 shows the cyclic voltammograms of Pd/Gr/PI and Pd/COOH-CNTs/PI catalysts in a solution of 0.5 mol/L HCOOH + 0.5 mol/L H_2SO_4 at room temperature. The forward scans of the CVs for the formic acid oxidation are characterized by a strong current peak A at 0.3 V and a shoulder peak B at 0.6 V. According to the previous Refs. [1,32,33,47] about Pd-based electrocatalysts for formic acid, peak A can be attributed to the direct oxidation of formic acid to form CO_2 (dehydrogenation path), while the peak B is related to the oxidation of the formic acid with the formation of intermediate CO generated from the dissociative adsorption step (dehydration path).

The oxidation process of formic acid can be expressed as two ways [48,49]: the direct oxidation way

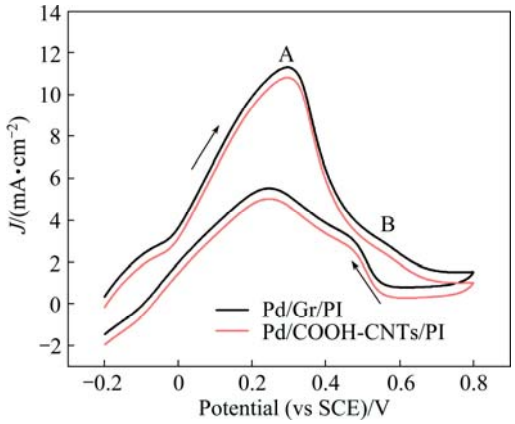

Fig. 7 Cyclic voltammograms for formic acid oxidation on Pd/COOH-CNTs/PI and Pd/Gr/PI catalysts recorded at 50 mV/s in 0.5 mol/L HCOOH + 0.5 mol/L H_2SO_4 solution

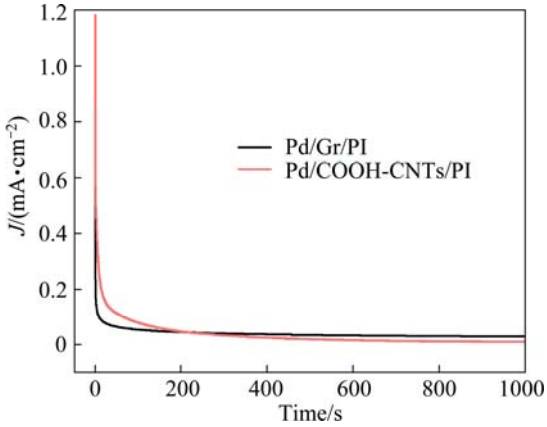

Fig. 8 Current density time plots for formic acid oxidation on Pd/COOH-CNTs/PI and Pd/Gr/PI catalysts measured at 0.3 V

(Pathway I) and indirect oxidation way (Pathway II). Pathway I:

$$HCOOH \rightarrow HCOO_{ad} + H^+ + e \rightarrow CO_2 + 2H^+ + 2e$$

Pathway II:

$$HCOOH \rightarrow CO_{ad} + H_2O \rightarrow CO_2 + 2H^+ + 2e$$

As can be seen, the peak potentials of the formic acid oxidation at the two catalysts are similar, but the current density of Pd/Gr/PI electrode is higher than that of Pd/COOH-CNTs/PI electrode. The oxidation peak current density for the Pd/Gr/PI catalyst is 11.3 mA/cm^2, which is higher than 10.6 mA/cm^2 for the Pd/COOH-CNTs/PI. This result indicates that the electrocatalytic activity of Pd/Gr/PI is obviously higher than that of Pd/COOH-CNTs/PI. This is because smaller metal particles and higher dense distribution desirably provide abundant catalytic sites and mean higher catalytic activity [31]. As a result, the Pd/Gr/PI catalysts have better catalytic performance for the oxidation of formic acid.

To evaluate the catalytic stability of catalysts, the chronoamperometry (CA) experiments were carried out in the solution of 0.5 mol/L H_2SO_4 + 0.5 mol/L HCOOH at a constant potential of 0.3 V, as shown in Fig. 8. The current densities for the formic acid oxidation reaction on the Pd/COOH-CNTs/PI and Pd/Gr/PI catalysts show the decay initially and reach a stable value after being polarized at 0.3 V for 600 s. The current decay for the HCOOH oxidation reaction indicates the slow deactivation of Pd-based electrocatalysts by the adsorption of CO or CO-like intermediates [4,5]. Nonetheless, the stable current density for the formic acid oxidation reaction on the Pd/Gr/PI is about 0.27 mA/cm^2, significantly higher than that on the Pd/COOH-CNTs/PI of 0.14 mA/cm^2. It indicates that the Pd/Gr/PI catalyst has a much better stability toward the process of formic acid catalytic oxidation. But compared with Refs. [50−52], the catalytic stability of Pd/C is greater than that of Pd/Gr/PI catalyst.

4 Conclusions

1) A novel Pd nano-electrocatalyst for DFAFCs was fabricated by electrodeposition on the surface of Gr/PI film.

2) The XRD and SEM analyses demonstrate that the particle size of Gr/PI composite membrane is smaller than that of COOH-CNTs/PI membrane, while the uniform and dense distribution of Pd micro-nanoparticles on the Gr/PI composite membrane is greater than that on the COOH-CNTs/PI membrane.

3) The electrochemical experiments demonstrate that the electrocatalytic activity and stability of Pd/Gr/PI are superior to those of Pd/COOH-CNTs/PI catalyst. This is because smaller metal particles and higher dense distribution desirably provide abundant catalytic sites and mean higher catalytic activity.

4) The flexible Gr/PI composite membrane is proved to be a better catalyst support than the COOH-CNTs/PI membrane. It is expected that further applications of the proposed electrodes will be explored in future.

References

[1] ZHU Y M, KHAN Z, MASEL R I. The behavior of palladium catalysts in direct formic acid fuel cells [J]. Journal of Power Sources, 2005, 139(1−2): 15−20.

[2] ZHU Y M, HA S Y, MASEL R I. High power density direct formic acid fuel cells [J]. Journal of Power Sources, 2004, 130(1−2): 8−14.

[3] WANG Shuang-yin, WANG Xin, JIANG San-ping. Controllable self-assembly of Pd nanowire networks as highly active electrocatalysts for direct formic acid fuel cells [J]. Nanotechnology, 2008, 19: 455602.

[4] YU X W, PICKUP P G. Mechanistic study of the deactivation of carbon supported Pd during formic acid oxidation [J]. Electrochemistry Communications, 2009, 11(10): 2012−2014.

[5] YU X W, PICKUP P G. Deactivation/reactivation of a Pd/C catalyst in a direct formic acid fuel cell (DFAFC): Use of array membrane electrode assemblies [J]. Journal of Power Sources, 2009, 187(2): 493−499.

[6] ZHANG Xin, SHI Xue-zhao, WANG Chun-ming. Electrodeposition of Pt micro-nanoparticles on carbon nanotubes-modified polyimide materials for electrocatalytic applications [J]. Catalysis Communications, 2009, 10(5): 610−613.

[7] KOU Huan-huan, JIA Ling-pu, WANG Chun-ming. Electrochemical deposition of flower-like ZnO micro-nanoparticles on a silver-modified carbon nanotube/polyimide membrane to improve its photoelectric activity and photocatalytic performance [J]. Carbon, 2012, 50(10): 3522−3529.

[8] JIANG Yi-min, KOU Huan-huan, LI Jia-jia, YU Sheng-jiao, DU Yong-ling, YE Wei-chun, WANG Chun-ming. Synthesis of ZnTe dendrites on multi-walled carbon nanotubes/polyimide nanocomposite membrane by electrochemical atomic layer deposition and photoelectrical property research [J]. Journal of Solid State Chemistry, 2012, 194: 336−342.

[9] SO H H, CHO J W, SAHOO N G. Effect of carbon nanotubes on mechanical and electrical properties of polyimide/carbon nanotubes nanocomposites [J]. European Polymer Journal, 2007, 43(9): 3750−3756.

[10] ZHU Bao-ku, XIE Shu-hui, XU Zhi-kang, XU You-yi. Preparation and properties of the polyimide/multi-walled carbon nanotubes (MWNTs) nanocomposites [J]. Composites Science and Technology, 2006, 66(3−4): 548−554.

[11] LIAO Y C, LIN C H, WANG S L. Direct white light phosphor: A porous zinc gallophosphate with tunable yellow-to-white luminescence [J]. Journal of the American Chemical Society, 2005, 127(28): 9986−9987.

[12] QU L W, LIN Y, HILL D E, ZHOU B, WANG W, SUN X F, KITAYGORODSKIY A, SUAREZ M, CONNELL J W, ALLARD L F, SUN Y P. Polyimide-functionalized carbon nanotubes: Synthesis and dispersion in nanocomposite films [J]. Macromolecules, 2004, 37(16): 6055−6060.

[13] SMITH J G, CONNELL J W, DELOZIER D M, LILLEHEI P T, WATSON K A, LIN Y, ZHOU B, SUN Y P. Space durable polymer/carbon nanotube films for electrostatic charge mitigation [J]. Polymer, 2004, 45(3): 825−836.

[14] GEIM A K, NOVOSELOV K S. The rise of graphene [J]. Nature Materials, 2007, 6: 183−191.

[15] ZHU Jun. Graphene production: New solutions to a new problem [J]. Nature Nanotechnology, 2008, 3: 528−529.

[16] LI D, KANER R B, Materials science: Graphene-based materials [J]. Science, 2008, 320(5880): 1170−1171.

[17] STANKOVICH S, DIKIN D A, DOMMETT G H B, KOHLHAAS K M, ZIMNEY E J, STACH E A, PINER R D, NGUYEN S T, RUOFF R S. Graphene-based composite materials [J]. Nature, 2006, 442: 282−286.

[18] NIYOGI S, BEKYAROVA E, ITKIS M E, MCWILLIAMS J L, HAMON M A, HADDON R C. Solution properties of graphite and graphene [J]. Journal of American Chemical Society, 2006, 128(24): 7720−7721.

[19] DIKIN D A, STANKOVICH S, ZIMNEY E J, PINER R D, DOMMETT G H B, EVMENENKO G, NGUYEN S T, RUOFF R S. Preparation and characterization of graphene oxide paper [J]. Nature, 2007, 448: 457−460.

[20] XU Chao, WANG Xin, ZHU Jun-wu. Graphene-metal particle nanocomposites [J]. Journal of Physical Chemistry C, 2008, 112(50): 19841−19845.

[21] SI Y C, SAMULSKI E T. Exfoliated graphene separated by platinum nanoparticles [J]. Chemistry of Materials, 2008, 20(21): 6792−6797.

[22] SEGER B, KAMAT P V. Electrocatalytically active graphene–platinum nanocomposites: Role of 2-D carbon support in PEM fuel cells [J]. Journal of Physical Chemistry C, 2009, 113(19): 7990−7995.

[23] YOO E J, OKATA T, AKITA T, KOHYAMA M, NAKAMURA J, HONMA I. Enhanced electrocatalytic activity of Pt subnanoclusters on graphene nanosheet surface [J]. Nano Letters, 2009, 9(6): 2255−2259.

[24] XU Yu-xi, BAI Hua, LU Ge-wu, LI Chun, SHI Gao-quan. Flexible graphene films via the filtration of water-soluble noncovalent functionalized graphene sheets [J]. Journal of American Chemical Society, 2008, 130(18): 5856−5857.

[25] SO H H, CHO J W, SAHOO N G. Effect of carbon nanotubes on mechanical and electrical properties of polyimide/carbon nanotubes nanocomposites [J]. European Polymer Journal, 2007, 43(9): 3750−3756.

[26] ZHU Bao-ku, XIE Shu-hui, XU Zhi-kang, XU You-yi. Preparation and properties of the polyimide/multi-walled carbon nanotubes (MWNTs) nanocomposites [J]. Composites Science and Technology, 2006, 66(3−4): 548−554.

[27] LIAO Yueh-chun, LIN Chia-her, WANG Sue-lein. Direct white light phosphor: A porous zinc gallophosphate with tunable yellow-to-white luminescence [J]. Journal of American Chemical Society, 2005, 127(28): 9986−9987.

[28] QU L W, LIN Y, HILL D E, ZHOU B, WANG W, SUN X F, KITAYGORODSKIY A, SUAREZ M, CONNELL J W, ALLARD L F, SUN Y P. Polyimide-functionalized carbon nanotubes: synthesis and dispersion in nanocomposite films [J]. Macromolecules, 2004, 37(16): 6055−6060.

[29] HUMMERS W S, OFFEMAN R E. Preparation of graphitic oxide [J]. Journal of American Chemical Society, 1958, 80(6): 1339−1339.

[30] LI J, KOU H, JIANG Y, LU D, ZHENG Z, WANG C. Electrochemical deposition of nano-semiconductor CuSe on multi-walled carbon nanotubes/polyimide membrane and photoelectric property researches [J]. Journal of Solid State Electrochemistry, 2012, 16(9): 3097−3103.

[31] MAIYALAGAN T, DONG X C, CHEN P, WANG X. Electrodeposited Pt on three-dimensional interconnected graphene as a free-standing electrode for fuel cell application [J]. Journal of Materials Chemistry, 2012, 22: 5286−5290.

[32] HA S, LARSEN R, ZHU Y, MASEL R I. Direct formic acid fuel cells with 600 $mA\cdot cm^{-2}$ at 0.4V and 22 °C [J]. Fuel Cells, 2004, 4(4): 337−343.

[33] HOU Lu-bing, DENG Hui-qiu, HU Wang-yu. Adsorption of hydrogen atoms on Pd(211), (311), and (511) stepped defective surfaces [J]. Transactions of Nonferrous Metals Society of China, 2006, 16(S): s820−s823.

[34] LIU Peng, LIU Guang-feng, CHEN Da-lin, CHENG Shao-yi, TANG Ning. Adsorption properties of Ag(I), Au(III), Pd(II) and Pt(IV) ions on commercial 717 anion-exchange resin [J]. Transactions of Nonferrous Metals Society of China, 2009, 19(6): 1509−1513.

[35] YANG T H, PYUN S I, YOON Y G. Hydrogen transport through Pd electrode: Current transient analysis [J]. Electrochimica Acta, 1997, 42(11): 1701−1708.

[36] TANG Jun-lei, ZUO Yu, TANG Yu-ming, XIONG Jin-ping. Composition and corrosion resistance of palladium film on 316L stainless steel by brush plating [J]. Transactions of Nonferrous Metals Society of China, 2012, 22(1): 97−103.

[37] TAN Rui-qin, GUO Yan-qun, ZHAO Jun-hua, LI Yue, XU Tie-feng, SONG Wei-jie. Synthesis, characterization and gas-sensing properties of Pd-doped SnO_2 nanoparticles [J]. Transactions of Nonferrous Metals Society of China, 2011, 21(7): 1568−1573.

[38] HOYER R, KIBLER L A, KOLB D M. The initial stages of palladium deposition onto Pt(111) [J]. Electrochimica Acta, 2003, 49(1): 63−72.

[39] SCHMIDT T J, MARKOVIC N M, STAMENKOVIC V, ROSS P N, ATTARD G A, WATSON D J. Surface characterization and electrochemical behavior of well-defined Pt-Pd (111) single-crystal surfaces: A comparative study using Pt(111) and palladium-modified

Pt(111) electrodes [J]. Langmuir, 2002, 18(18): 6969−6975.
[40] ARENZ M, STAMENKOVIC V, SCHMIDT T J, WANDELT K, ROSS P N, MARKOVIC N M. The effect of specific chloride adsorption on the electrochemical behavior of ultrathin Pd films deposited on Pt(111) in acid solution [J]. Surface Science, 2003, 523(1−2): 199−209.
[41] KIBLER L A, KLEINERT M, RANDLER R , KOLB D M. Initial stages of Pd deposition on Au(hkl). Part I: Pd on Au(111) [J]. Surface Science, 1999, 443(1−2): 19−30.
[42] NAOHARA H, YE S, UOSAKI K. Electrochemical deposition of palladium on an Au (111) electrode: Effects of adsorbed hydrogen for a growth mode [J]. Colloids and Surfaces A: Physicochemical and Engineering Aspects, 1999, 154(1−2): 201−208.
[43] PASTI I A, MENTUS S V. Halogen adsorption on crystallographic (111) planes of Pt, Pd, Cu and Au, and on Pd-monolayer catalyst surfaces: Firstprinciples study [J]. Electrochimica Acta, 2010, 55(6): 1995−2003.
[44] SCHARIFKER B. Theoretical and experimental studies of multiple nucleation [J]. Electrochimica Acta, 1983, 28(7): 879−889.
[45] WANG Rong-fang, LIAO Shi-jun, JI Shan. High performance Pd-based catalysts for oxidation of formic acid [J]. Journal of Power Sources, 2008, 180(1): 205−208.
[46] WANG Zai-hua, DU Yong-ling, ZHANG Feng-yuan, ZHENG Zhi-xiang, ZHANG Yu-zhen, WANG Chun-ming. High electrocatalytic activity of non-noble Ni-Co/graphene catalyst for direct ethanol fuel cells [J]. Journal of Solid State Electrochemistry, 2013, 17(17): 99−107.
[47] SAMJESKE G, MIKI A, YE S, OSAWA M. Mechanistic study of electrocatalytic oxidation of formic acid at platinum in acidic solution by time-resolved surface-enhanced infrared absorption spectroscopy [J]. Journal of Physical Chemistry, 2006, 110(33): 16559−16566.
[48] YI Qing-feng, XIAO Xing-zhong, LIU Yun-qing. Hydrothermal synthesis of titanium-supportted nanoporous palladium−copper electrocatalysts for formic acid oxidation and oxygen reduction reaction [J]. Transactions of Nonferrous Metals Society of China, 2013, 23(4): 1184−1190.
[49] WU Qiu-mei, RUAN Jian-ming, ZHOU Zhong-cheng, SANG Shang-bin. Effect of preparation routes on activity of Ag−MnOx/C as electrocatalysts for oxygen reduction reaction in alkaline media [J]. Transactions of Nonferrous Metals Society of China, 2015, 25(2): 510−519.
[50] MAIYALAGAN T, NASSR A B A, ALAJE T O, BRON M, SCOTT K. Three-dimensional cubic ordered mesoporous carbon (CMK-8) as highly efficient stable Pd electro-catalyst support for formic acid oxidation [J]. Journal of Power Sources, 2012, 211: 147−153.
[51] MAIYALAGAN T, WANG X, MANTHIRAM A. Highly active Pd and Pd–Au nanoparticles supported on functionalized graphene nanoplatelets for enhanced formic acid oxidation [J]. RSC Advances 2014, 4: 4028−4033.
[52] KANNAN P, DOLINSKA J, MAIYALAGAN T, OPALLO M. Facile and rapid synthesis of Pd nanodendrites for electrocatalysis and surface-enhanced Raman scattering applications [J]. Nanoscale, 2014, 6: 11169−11176.

Pd 微纳米粒子在石墨烯/聚酰亚胺薄膜上的电沉积及其电催化氧化甲酸

张 焱，王 琴，叶为春，李佳佳，王春明

兰州大学 化学化工学院，兰州 730000

摘 要：利用电化学沉积法在柔韧的石墨烯/聚酰亚胺(Gr/PI)复合膜上制备一种新的花状、微纳结构的 Pd 电催化剂。作为对比研究，同时在羧基化碳纳米管/聚酰亚胺(COOH-CNTs/PI)上制备 Pd 微纳米粒子催化剂。对合成的 Pd/Gr/PI 和 Pd/COOH-CNTs/PI 进行 X 射线衍射(XRD)和扫描电子显微镜(SEM)分析。XRD 和 SEM 分析结果表明：当沉积条件相同时，相对于在 COOH-CNTs/PI 膜上制备的 Pd 微纳米粒子，在 Gr/PI 复合膜上电沉积得到的 Pd 微纳米粒子尺寸更小，分布密度更大，且分布更均匀。通过循环伏安法(CV)和计时电流法(CA)研究这两种催化剂对甲酸的电催化氧化性能。结果表明：在 Gr/PI 电极上沉积得到的 Pd 的催化效率更高、稳定性更好。这是由于在 Gr/PI 电极上沉积得到的 Pd 颗粒尺寸更小，分布密度更大，催化活性点位更多，因而对甲酸的催化氧化效果更好。

关键词：Pd 微纳米粒子；Gr /PI 薄膜；COOH-CNTs/PI 薄膜；电催化氧化；甲酸；电化学沉积

(Edited by Mu-lan QIN)